

AD-A103 125

FOREIGN TECHNOLOGY DIV WRIGHT-PATTERSON AFB OH
ACTA MECHANICA SINICA (SELECTED ARTICLES), (U)
JUL 81 W XILANG, X CHANGSHENG, C XI
UNCLASSIFIED FTD-ID(RST)-0413-81

F/6 20/4

1 OF 1
AD A
103-24

END
DATE FILMED
9-81
DTIC

AD A103125

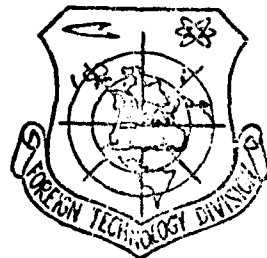
2
B-1

FTP-ID(RC)T-0413-81

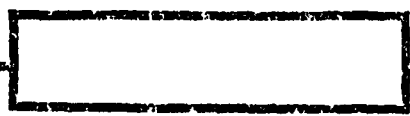
FOREIGN TECHNOLOGY DIVISION



ACTA MECHANICA SINICA
(Selected Articles)



Approved for public release;
distribution unlimited.



81 8 20 089

FTD-ID(RS)T-0413-81

EDITED TRANSLATION

FTD-ID(RS)T-0413-81

24 July 1981

MICROFICHE NR: FTD-81-C-000676

ACTA MECHANICA SINICA (Selected Articles)

English pages: 28

Source: Acta Mechanica Sinica, Nr. 4, 1978,
pp. 326-339

Country of origin: China

Translated by: SCITRAN
F33657-78-D-0619

Requester: FTD/TQTA

Approved for public release; distribution
unlimited.

THIS TRANSLATION IS A RENDITION OF THE ORIGINAL FOREIGN TEXT WITHOUT ANY ANALYTICAL OR EDITORIAL COMMENT. STATEMENTS OR THEORIES ADVOCATED OR IMPLIED ARE THOSE OF THE SOURCE AND DO NOT NECESSARILY REFLECT THE POSITION OR OPINION OF THE FOREIGN TECHNOLOGY DIVISION.

PREPARED BY:

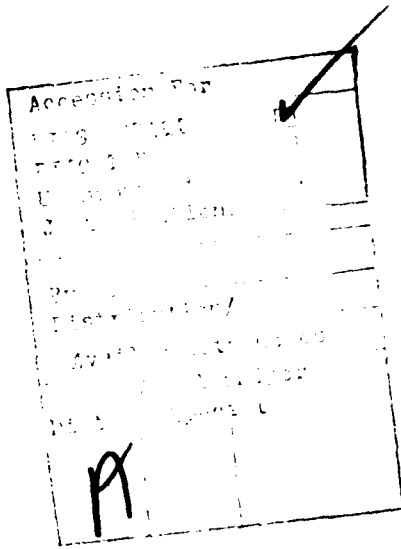
TRANSLATION DIVISION
FOREIGN TECHNOLOGY DIVISION
WP-AFB, OHIO.

FTD-ID(RS)T-0413-81

Date 24 Jul 1981

TABLE OF CONTENTS

Reduction Theory and Experimental Investigation of in Slit Injected Polymer Solution Under High Reynold Numbers, by Wang Xiliang, Xia Changsheng.....	1
Simple Analysis of a Centrifugal Nozzle With Annular Cross-Sectional Outlet, by Chen Xi.....	12



REDUCTION THEORY AND EXPERIMENTAL INVESTIGATION OF IN SLIT
INJECTED POLYMER SOLUTION UNDER HIGH REYNOLD NUMBERS

Wang Xiliang Xia Changsheng

The addition of a small amount of drag-reducing polymer in near-wall flow may greatly reduce the sliding friction. In engineering we are interested in the theory and experimentation of high Reynold number slit injection of drag-reducing polymer. Our results are presented below.

1. Differential relations of wall shear stress of slit-injected drag-reducing polymer solution in flow around a streamlined body of revolution.

This method is based on the velocity distribution of the joint boundary layer in references (4) and (5). The equation is

$$u^+ = \frac{u}{v_*} = A \ln y^+ + B + b a y^+ + \Delta B \quad (1)$$

where u is the velocity component along x direction in the boundary layer; $y^+ = v_* y / v$; $v_* = \sqrt{\tau_w / \rho}$ is the shear velocity, τ_w is the wall shear stress, ρ is the density; A , B are constants, with $A = 2.5$ and $B = 5.5$; $a = \frac{v}{\tau_w v_*} \frac{dp}{dx}$, v is the kinematic viscosity, p is the pressure;

$\Delta B = \Gamma \ln (v_* / v_{*cr})$, $\Gamma = \Gamma(c)$ is related to the concentration c , v_{*cr} is the shear velocity at the onset of drag-reduction.:

$$b = \begin{cases} 0, & \text{for zero or negative pressure gradient} \\ 0.6, & \text{for positive pressure gradient.} \end{cases}$$

The continuity equation of the flow around a body of revolution is

$$\frac{\partial(ru)}{\partial x} + \frac{\partial(rv)}{\partial y} = 0 \quad (2)$$

When normal stress is neglected, the equation of motion is

$$u \frac{\partial u}{\partial x} + v \frac{\partial u}{\partial y} = - \frac{1}{\rho} \frac{\partial p}{\partial x} + \frac{1}{\rho r} \frac{\partial(r\tau)}{\partial y} \quad (3)$$

where x and y are respectively the tangential and normal direction of the object profile in the meridian plane; $r = r_0 + y \cos \phi$, ϕ is the angle between the x direction and the axis, r_0 is the distance from a point on the object surface to the axis. (Figure 1).

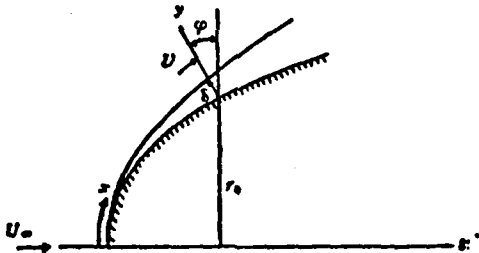


Figure 1. Coordinates of the body of revolution.

We assume the boundary layer to be a thin boundary layer with thickness $\delta \ll r_0$.

Integrating equation (2), we get

$$v = -yu^+ \frac{dv^+}{dx} - y^+ \left[\frac{b}{2} \frac{dy^+}{dx} + \frac{d(\Delta B)}{dx} \right] - \frac{v}{r} \frac{dr}{dx} y^+ \left(u^+ - \frac{b y^+}{2} - A \right) \quad (4)$$

$$\frac{\partial u}{\partial x} = \frac{\partial}{\partial x} [v_* (A \ln y^+ + b a y^+ + B + \Delta B)] = \frac{d v_*}{d x} (u^+ + A + b a y^+) + \left[b y^+ \frac{d a}{d x} + \frac{d(\Delta B)}{d x} \right] v_* \quad (5)$$

Substituting equations (4) and (5) into (3) and noticing that

$$u^+ v_* \frac{d v_*}{d x} y^+ \left(\frac{A}{y^+} + b a - \frac{d u^+}{d y^+} \right) = 0, \text{ 得到}$$

then we get

$$u^{+2} v_* \frac{d v_*}{d x} + b v_*^2 \frac{d a}{d x} \left[u^+ y^+ - \frac{1}{2} y^{+2} \frac{d u^+}{d y^+} \right] - \frac{1}{r} \frac{d r}{d x} v_*^2 y^+ \left(u^+ - \frac{b a y^+}{2} - A \right) \frac{d u^+}{d y^+} + v_*^2 \left(u^+ - y^+ \frac{d u^+}{d y^+} \right) \frac{d(\Delta B)}{d x} = - \frac{1}{\rho} \frac{d p}{d x} + \frac{1}{\rho r} \frac{\partial(r \tau)}{\partial y} - U \frac{d U}{d x} + \frac{v_*}{\mu} \frac{\partial \tau}{\partial y^+}$$

Integrating the above equation from 0 to $\delta^+ = v_* \delta / v$ we get

$$v_* \frac{d v_*}{d x} G + b v_*^2 \frac{d a}{d x} H - \frac{1}{r} \frac{d r}{d x} v_*^2 \delta^+ \left[\left(A + \frac{b a \delta^+}{2} \right) \sigma - \frac{1}{3} b^2 a^2 \delta^{+2} - \frac{3}{2} A b a \delta^+ - 2 A^2 \right] + v_*^2 \delta^+ (\sigma - b a \delta^+ - 2 A) \frac{d(\Delta B)}{d x} - U \frac{d U}{d x} \delta^+ - \frac{v_*}{\mu} \tau_w \quad (6)$$

where U is the flow velocity at the outer edge of the boundary layer; μ is the viscosity;

$$\begin{aligned} \sigma &= u^+ \Big|_{y^+ = \delta^+} = \frac{U}{v_*} \\ G &= \int_0^{\delta^+} u^{+2} dy^+ = \delta^+ \left[(\sigma - A)^2 + A^2 - b a \delta^+ \left(\sigma - \frac{1}{3} b a \delta^+ - \frac{3}{2} A \right) \right] \\ H &= - \frac{\sigma \delta^{+2}}{2} + 2 \int_0^{\delta^+} y^+ u^+ dy^+ = \frac{\delta^{+2}}{2} \left(\sigma - A - \frac{2}{3} b a \delta^+ \right) \end{aligned}$$

Let the stiffness approach infinity in equation (6) and let $V = U/U_\infty$, $\tilde{x} = x/L$, $\tilde{r} = r/L$, where U_∞ is the flow velocity at infinity. L is the length of the body. Finally we obtain the differential relation for the shearing stress of the body of revolution with slit injection.

$$\begin{aligned}
 (G - 3baH)\sigma' + \frac{V'}{V}\sigma(\sigma'\delta^+ - G) - \sigma'\left(\frac{1}{V}\right)''\frac{bH}{R_L} \\
 + \frac{\tilde{r}'}{\tilde{r}}\sigma\delta^+ \left[\left(1 + \frac{ba\delta^+}{2}\right)\sigma - \frac{1}{3}b^2\sigma^2\delta^{+2} - \frac{3}{2}Ab\sigma\delta^+ - 2A^2 \right] \\
 - \sigma\delta^+(\sigma - 2A - ba\delta^+) (\Delta B)' = R_L V
 \end{aligned} \tag{7}$$

in which the ' and the " represent the first and second order derivative wrt \bar{x} ;

$$\begin{aligned}
 R_L &= U_L L / \nu; \\
 (\Delta B)' &= \frac{I'}{I}(\Delta B) + I\left(\frac{V'}{V} - \frac{\sigma'}{\sigma}\right)
 \end{aligned} \tag{8}$$

2. Discussion on the differential relation of the shearing stress.

1) when $B=0$, equation (7) is the shearing stress differential relation for the flow around the body of revolution without the additive.

2) From equation (8), we have $(\Delta B)' = (-I\sigma')/\sigma$, in plane uniform solution flow. Equation (7) becomes

$$\begin{aligned}
 \sigma^+ [(\sigma - A)^2 + A^2 + I(\sigma - 2A)]\sigma' = R_L V \text{ or } \delta^+ [(\sigma - A)^2 \\
 + A^2 + I(\sigma - 2A)] \frac{d\sigma}{dR_s} = 1
 \end{aligned} \tag{9}$$

Equation (9) has the solution

$$R_s = e^{-\frac{I}{A}}(\sigma_{\infty})^{-\frac{I}{A}} \left[\sigma_{\left(\frac{I}{A}+1\right)} + (I + 2A)\sigma_{\left(\frac{I}{A}+1\right)} - 2A(I - A)\sigma_{\frac{I}{A}} \right] \tag{10}$$

when I/A is an integer.

$$\text{Here } \sigma_0 = A e^{\frac{I}{A}}, \sigma_{\frac{I}{A}} = A \left(\sigma^{\frac{I}{A}} e^{\frac{I}{A}} - \frac{I}{A} \sigma_{\left(\frac{I}{A}-1\right)} \right)$$

When $I/A = 0$, this is then the solution for the flow around the body without the additional plane. The plane drag

$$\text{coefficient } (2) \text{ is } C_1 = \frac{2}{R_L} \int_0^{R_L} \frac{dR_s}{\sigma^2} = \frac{2}{R_L} \left[\frac{1}{\sigma} \int_0^{\sigma^+} u^+ (\sigma - u^+) dy^+ \right]$$

For our model, we have

$$C_f = \frac{2A\delta^+(\sigma - 2A)}{R_L \sigma} \quad (11)$$

Figure 2 shows the relational curves of C_f to the Reynold number Re for poly(ethylene oxide) solution of various concentrations $\Gamma/A = 1, 2, 5$ and for pure water $\Gamma/A = 0$. Here $U_\infty = 10$ m/s, $V_* = 0.023$ m/s.

3) For the case of pure water, the separation condition for the flow around a body is $G - 3baH = 0$; in the presence of drag-reducing polymer, the separation point condition is

$$G - 3baH + \Gamma\delta^+(\sigma - 2A - bA\delta^+) = 0$$

The extra third term is usually greater than zero. When separation exists, we may interpret this as moving the separation

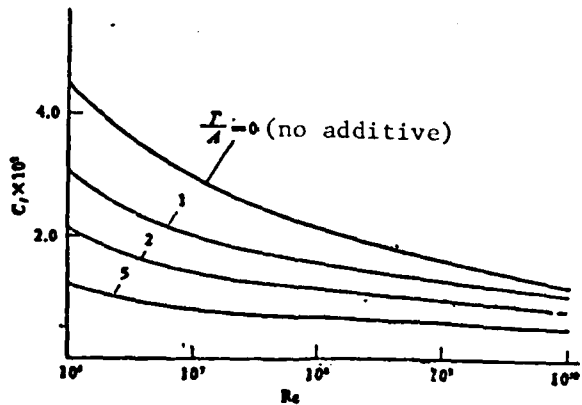


Figure 2. Curve of plane viscosity for uniform solution

point further to the rear (σ, δ^+, G and H also change with additive). In practice, the curve for wall shear stress coefficient $\tau_w/\rho U^2 = 1/\sigma^3$ is calculated from equation (7). In the case of pure water, the tail of the body of revolution

makes σ' increase rapidly and $\tau_w/\rho U^2$ curve decrease since V'/V and \bar{r}'/r are both large negative numbers. When $\tau_w/\rho U^2 \rightarrow 0$, separation occurs. With additive, because of the extra term

$\Gamma \delta^* (\sigma - 2A - b\sigma \delta^*)$, the coefficient of σ' increases so that the fall-off phenomenon of the curve due to V'/V and \bar{r}'/\bar{r} is moderated, delaying the occurrence of separation.

4) It is very important in solving equation (7) to establish the wall concentration relation along the longitudinal direction and to derive from which the expression for $(\Delta B)'$. When we assume that the diffusion of the slit injected polymer at the boundary layer is similar to the diffusion law of the line source at the turbulent boundary layer, the final stage wall concentration

$$C_w(x) = g/0.55 \delta U \quad (12)$$

where g is the unit length injection rate.^[7] When Γ is taken to be directly proportional to C_w , equation (12) may be re-written as

$$\Gamma \sigma \delta^* = \text{constant} \quad (13)$$

From (13) with the consideration of the expressions for σ and ΔB , we can derive

$$(\Delta B)' = [K_1(\sigma + \Gamma + \Delta B - 3b\sigma \delta^*) - (\Gamma + \Delta B)] \frac{\sigma'}{\sigma} + [\Gamma - K_1(\Gamma - 2b\sigma \delta^*)] \frac{V'}{V} - K_1 b\sigma \delta^* \frac{V''}{V'} \quad (14)$$

where

$$K_1 = \frac{\Delta B}{\Delta B - A - b\sigma \delta^*}$$

3. Experiment on drag-reduction and wall concentration measurement for slit injection on a plane and on a body of revolution.

1) The measuring procedure

The model used in this experiment consists of a plane and a body of revolution. The length of the plane is 3.0 m and its thickness is 25 mm, with both ends trimmed sharp. There is a slit of width 0.8 mm at an angle of about 30° with the surface from the front end of the plane. During the experiment the part of the plane under the water line is 0.338 m. Six sampling slits of width 0.25 mm and effective length 30 - 35 mm are placed along the longitudinal direction. Their positions are tabulated in tables 1 and 2. The body of revolution has a length of 5.463 m. There is an annular injection slit of width about 0.8 mm and at an angle of about 7° with the surface at a distance of 0.439 m from the front end of the body. Seven sampling slits similar to those for the plane are placed along the longitudinal direction. We used the vacuum suction sampling method with a sampling rate of about $0.3 \text{ cm}^3/\text{s.cm.}$ For concentration determination we used the turbidity method: 1 cc 50% sulphuric acid and 1 cc 1% phosphorous molybdenum acid are added to 10 cc of the solution and the mixture is shaken until the mixing is uniform. 10 minutes is allowed for the solution to settle and then its optical density is measured with a Model 72 photometer. The drag-reducing agent is poly(ethylene oxide) with a molecular weight of about 3 million. The injection concentration is approximately 500 ppm and the injection rates for the plane and the body of revolution respectively are 1 kg/s and 0.74 kg/s.

2. Experimental results

Figures 3 and 4 represent respectively the experimental results of the slit injection for the plane and for the body of revolution. The experimental Reynold numbers are respectively $3 \times 10^6 - 2.7 \times 10^7$ and $5.5 \times 10^6 - 5.4 \times 10^7$. The largest reduction of drag coefficient is approximately 45% and 39%. For constant injection rate and injection concentration, the

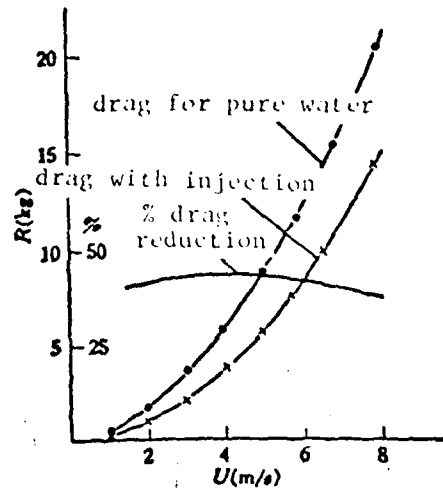


Figure 3. Drag experiment curves of the plane for pure water and for slit injection of 500 ppm poly(ethylene oxide).

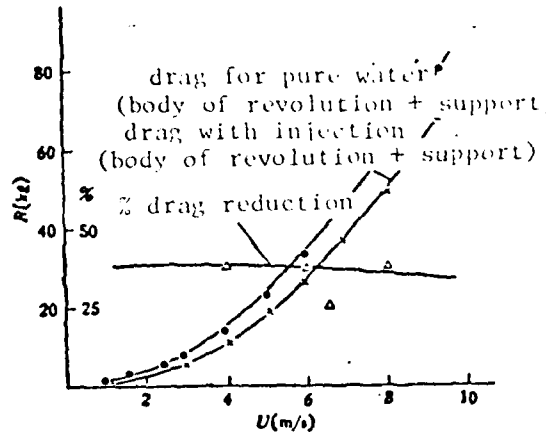


Figure 4. Drag experiment curve of a body of revolution for slit injection of poly(ethylene oxide) solution and the comparison between theoretically calculated percentage drag reduction and the experimental results.

drag reduction decreases slightly with increasing velocity. This decrease is more pronounced for the plane than for the body of revolution because at high velocity there is less water immersgence for the plane due to the free surface effect.

The measured results of the wall concentration for the plane and for the body of revolution with slit injection are tabulated in Table 1 and Table 2 in which V is the flow speed (m/s), Q_j is the injection rate (kg/s), C_j is the injection concentration (ppm), C_w is the wall concentration (ppm), and x is the distance (m) from the front end. * indicates a higher concentration because the sampling bottle was not thoroughly cleaned after sampling for the $C_j = 1000$ ppm case.

The results for the wall concentration shows that the variation of wall concentration is larger near the slit outlet.

The wall concentration within 1.5 m from the slit is bigger than the saturated concentration of 25 ppm for drag reduction. There seems to be a region with relatively small variation in the concentration for a fairly long distance toward the rear, especially for the case of the body of revolution. It is difficult to reduce the wall concentration to an expression used in reference [3], especially for the region where $C_w/C_j = 1$. For the case as described in our paper, the wall concentration must be affected by the injection angle, the pressure and the surface curvature of the object.

Table 1 Wall Concentration for the plane with injection

conditions of injection		$V = 3.540$	$V = 5.106$	$V = 6.561$	$V = 7.820$	$V = 3.480$
C_w	x	$Q_j = 1.0$				
		$C_j = 536$	$C_j = 536$	$C_j = 536$	$C_j = 536$	$C_j = 1000$
0.236	420	476	440	424	862	
0.375	310	364	360	340	832	
0.681	200	272	204	157	562	
1.170	37.2	62.4	60	84	66	
2.202	31.3	12.7	14.3	13.1	10.1	
2.757	8.5	8.4	8.8	9.6	14.3	

Table 2 Wall concentration for the body of revolution with injection.

conditions of injection		$V = 4.060$	$V = 5.989$	$V = 6.962$	$V = 4.230$	$V = 4.055$	$V = 4.026^*$
C_w	x	$Q_j = 0.735$	$Q_j = 0.735$	$Q_j = 0.735$	$Q_j = 0.735$	$Q_j = 0.89$	$Q_j = 0.735$
		$C_j = 536$	$C_j = 588$	$C_j = 588$	$C_j = 1000$	$C_j = 588$	$C_j = 588$
0.454	104	200	233	793	420	462	
0.895	116	112	100	530	208	182	
1.397	114	104	110	246	136	110	
2.199	12.6	5.9	7.7	118	17.8	13.8	
2.998	8.1	5.5	6.7	14.7	13.6	11.7	
3.798	6.1	5.4	6.2	8.5	11.0	9.4	
4.700	6.3	6.0	6.2	8.5	10.0	9.3	

4) Comparison between theoretical calculation and experimental result

We carried out theoretical calculation for the body of revolution of length 5.463 m at velocities = 4, 6 and 8 m/s. The method in reference [8] was used for potential flow calculation. Runge-Kutta method was used to solve quation (7). When we took $C_w = \sigma / 0.558U$ and used equation (14) for (ΔB) as derived from it, the value for the drag reduction was somewhat lower than the actual value. In this paper we used in our calculation the average value of the wall concentration as determined by the experiment. The initial value was determined from $\sigma = A \ln \delta^* + B \delta^* + B + \Delta B$ where the boundary layer thickness $\delta = 0.0598s / (\log \text{Res} - 3.17)$, s is the arc length, and the corresponding Reynold number is $\text{Res}^{(9)}$. In the calculation, $\Delta B = C_w \log \frac{U_w}{U_{\infty}}$. When the velocity was 4m/s, the curves for the shear stress coefficient $\tau_w / \rho U^2 = 1/\sigma^2$ are shown in Figure 5 for pure water and for poly(ethylene oxide) with injection concentration 500 ppm.

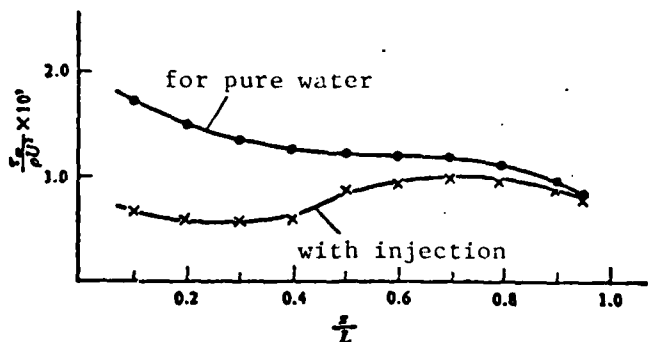


Figure 5. Theoretically calculated curves of $\tau_w / \rho U^2$ for water and for solution.

Integrating along the surface for wall shear stress for water and for solution as well as for their difference, we obtain respectively the value for drag coefficient and drag

reduction. We also plotted the theoretically calculated percentage drag reduction in Figure 4 from which one can see that the theoretical calculation basically agrees with experimental result. This method may be used to predict the calculated drag reduction for a body of revolution with injection. Strictly speaking, when applying Meyer's model to external flow, and in particular to external flow with uniform concentration, the assumed form $\Delta B = \Gamma(c_w) \ln \frac{v_{\infty}}{v_{scr}}$ requires proof by direct measurement.

The terms in equation (7) of this paper have clear physical meaning and its calculation is simple. Therefore it furnished us a method to calculate drag reduction that basically agrees with experimental result.

We are obliged to Comrades Zhou Dexiang and Wang Gueiqin for supplying data from concentration measurement.

REFERENCES

- [1] Test, F. L., *J. Hydraulics*, 8, 2 (1974), 45-46.
- [2] Sedov, L. I., Vasetskaya, N. G. and Ioselovich, V. A., *Calculation of Turbulent Boundary Layer with Polymer Additives*, ICDR, Cambridge, England, Sept. 1974 B6-69.
- [3] Frumen, D. H. and Tulin, M. P., *JSE*, 20, 3 (1976), 171-180.
- [4] White, F. M., *Trans. ASME, Series D*, 91, 3 (1969), 371-378.
- [5] Meyer, W. A., *AICHEJ*, 12, 3 (1966), 522-525.
- [6] Graville, P. S., *The Calculation of Viscous Drag of Bodies of Revolution*, DTMB, R849 (1953).
- [7] Porch, M. and Hsu, K. S., *J. Hydraulics*, 6, 1 (1972).
- [8] Young, A. D. and Owen, P. R., *A Simplified Theory for Streamline Bodies of Revolution and its Application to the Development of High Speed Shapes*, ABC, R and M-2071 (1943).
- [9] Graville, P. S., *ISP*, 7, 69 (1960).

SIMPLE ANALYSIS OF A CENTRIFUGAL NOZZLE WITH
ANNULAR CROSS-SECTIONAL OUTLET

Chen Xi, Qinghua University

Notation: r_c , R , f_1 , $A = \pi R r_c / \psi f_1$ denotes respectively the outer radius of the centrifugal nozzle outlet, the vortex flow arm through which the fuel enters the vortex flow chamber, the inlet cross-sectional area, and the geometrical characteristic parameter; G' , μ , α , r_v , $\phi = 1 - (r_v/r_s)^2$ denote respectively the discharge rate of the simple centrifugal nozzle, the discharge coefficient, the outlet spray angle, the radius of air vortex, and the coefficient of effective outlet cross-section; G , μ , α , r , $\phi = 1 - (r/r_s)^2$ denote respectively the discharge rate of a centrifugal nozzle with annular cross-sectional outlet, the discharge rate coefficient, the outlet spray angle, the radius of the central cylinder, and the coefficient of annular outlet cross-section area; w , w_α , w_T , w_o denote respectively the total velocity at an arbitrary point r in the outlet cross-sectional area, the axial velocity, the tangential velocity and the total velocity when the pressure energy is completely converted into kinetic energy; p_o , p_s , p'_s denote respectively the oil pressure in front of the nozzle, the static pressure at the point where the centrifugal nozzle with annular outlet $r = r_s$, and the static pressure at the point where the simple centrifugal nozzle outlet $r = r_s$ (all are residual pressures relative to the ambient medium); ψ is the corrected discharge coefficient of the nozzle inlet passage and the coefficient of flow column shape change as the fuel enters into the vortex chamber, γ is the fuel weight, and g is the gravitational acceleration; the subscripts 1, 2, 3 denote respectively the results corresponding to the 3 different assumptions on p_s , s denotes the value at the point where $r = r_s$ or denotes the value of the annular outlet cross-sectional area, the sub-

script v denotes the value at the air vortex boundary; the superscript denotes the value corresponding to the case when the central cylinder is absent (simple centrifugal nozzle).

1. Centrifugal nozzles are widely used in power, aeronautic, chemical and metallurgical industries. The operational characteristics of the simple centrifugal nozzle has long been analysed by G. N. Abramovich [1] (we shall refer to it as A's theory). A large amount of experimental and theoretical materials from analysis have been accumulated. Ordinarily for furnace nozzles the experimental results do not deviate from A's theory significantly. This shows that the theory basically reflects the operational characteristics of the centrifugal nozzle. Therefore it remains to be the foundation of industrial calculations, and forms the point of departure for the calculation of more complicated nozzles with structures. [2]

To increase the range of centrifugal nozzle flow rate regulation, various structures involving such forms as fuel return, nozzle outlet cross-sectional area regulation, or co-axial placement of principal and auxilliary nozzles, etc. may be used [2,3]. In several of these cases, we encounter the centrifugal nozzle with annular outlet cross-section. Research on this kind of nozzles at present is still rather scanty.

In this paper we shall analyse a nozzle which relies on a change in the cross-sectional area of its annular outlet to regulate the fuel rate (Figure 1). Its only difference from the simple centrifugal nozzle is in the installation of a conical-shaped pin rod at the center. The fuel rate is regulated by moving the pin rod forward or backward so as to change the size of the annular cross-sectional area of the outlet nozzle, while keeping the fuel pressure constant. The typical result of experiments performed on the nozzle test platform

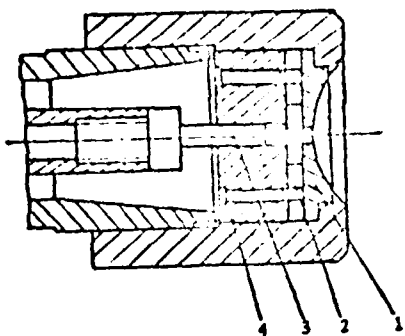


Figure 1. Centrifugal nozzle with adjustable outlet cross-sectional area.

1. Orifice, 2. Vortex flow disc, 3. Central pin rod (can be moved forward or backward), 4. fuel-separation ring.

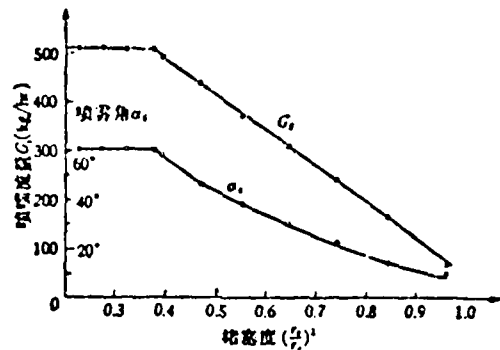


Figure 2. Regulation characteristics of centrifugal nozzle with adjustable outlet cross-sectional area.

4. Rectangular tangential slots of dimension 1.87×2.595
 $A = 1.575$

is shown in Figure 2. From Figure 2 we can see that when the pin rod is being moved forward and the blockage of the outlet is being gradually increased, there is an initial stage during which the nozzle flow rate and the spray angle are practically unaffected by the blockage. They only show significant change when the degree of blockage is greater than a certain value: a rapid decrease with increasing blockage. Similar experimental result is obtained in reference [3].

2. For conciseness, we shall base our analysis in this paper on the theory of an ideal fluid in a simple centrifugal nozzle. However, in order to obtain better accuracy in our calculation with the theoretical formulae, we shall first make some modifications to the original A's theory on simple centrifugal nozzles.

In a simple centrifugal nozzle, owing to the centrifugal effect produced by the tangential entry of the fuel oil, the fuel does not flow through every part of the nozzle outlet

cross-sectional area. Instead, an air vortex is formed near the axis of the nozzle, with the coefficient of effective cross-sectional area $\phi = 1 - (r_a/r_s)^2 \leq 1$. The magnitude of ϕ is determined by A , the geometrical characteristic parameter of the nozzle at infinite stiffness:

$$A = \frac{\pi R r_s}{\phi h_s} \quad (1)$$

The geometrical characteristic parameter A of the nozzle, the coefficient of effective outlet cross-section area ϕ , the nozzle discharge coefficient and the spray angle α are related as follows:

$$A = \frac{1 - \phi}{\phi \sqrt{\frac{\phi}{2}}} \quad (2)$$

$$\mu = \phi \sqrt{\frac{\phi}{2 - \phi}} \quad (3)$$

$$\alpha = 2 \sin^{-1} \left(\frac{2A\mu}{1 + \sqrt{1 - \phi}} \right) \quad (4)$$

We differ from the original A's theory on only two counts: one is that we introduced in equation (1) the correction coefficient to correct the effect introduced by the fact that the discharge coefficient in the tangential entrant passage is not equal to 1 and the fact that the fuel shape deforms as the fuel enters the vortex flow chamber, $\phi \leq 1$; two is that we have taken into consideration the effect on the spray angle when the static pressure of the fuel is transformed into axial velocity at the nozzle outlet. Let $\sin(\alpha/2) = (\text{average tangential velocity at the nozzle outlet}) / (\text{the total velocity when the pressure before the nozzle is completely transformed into kinetic energy})$.

Table 1 compares the experimental results with the results calculated from equations (1) - (4). The average value and

upper and lower error limits for 16 nozzles are

$$\frac{\mu_{\text{EX}}}{\mu_{\text{AN}}} = 1.004 \pm 0.05, \quad \frac{\sigma_{\text{EX}}}{\sigma_{\text{AN}}} = 1.015 \pm 0.17$$

while the ratio of the experimental results with that from the original A's theory are

$$\frac{\mu_{\text{EX}}}{\mu_{\text{AN}} \text{ (A's)}} = 0.88 \pm 0.14, \quad \frac{\sigma_{\text{EX}}}{\sigma_{\text{AN}} \text{ (A's)}} = 0.87 \pm 0.16$$

Hence the modified or corrected formulae (1) - (4) agrees better with experiment than the original A's theory.

The nozzles listed in Table 1 all came from actual production and therefore may be regarded as representative. For the 2 nozzles used in our experiment, when ψ is taken to be 0.8, the calculated results from (1) - (4) also agreed well with experiment. When the central pin rod is ineffective (equivalent to a simple centrifugal nozzle), for the nozzle with 3 tangential circular holes and $A = 1.123$, the discharge coefficient has a computational value of 0.411, the experimental value being 0.371, computed value for the spray angle is 69.5° , the experimental value being 61° ; For the nozzle with 4 rectangular tangential slot and $A = 1.575$, the computed value for discharge coefficient is 0.337, the experimental value being 0.335, the computed value for the spray angle is 78.7° , the experimental value being 72° .

In Table 1, we take $\psi = 0.8$ to compute A . Strictly speaking, ψ should be dependent upon the structure of the nozzle and its state of mechanical processing. For simplicity, we shall take $\psi = 0.8$ in all the subsequent analysis.

For computation of equations (2) and (3) it is possible to use the curve in reference [1]. Equation (2) - (4) may also

Table 1.

(1) 管道編號	1	2	3	4	5	6	7	8	9	10	13	15	16	22	24	25	(2) $\frac{1}{4} \pi r_s^2$
(3) 几何特征																	
$A = \frac{\pi r_s^2}{4}$	1.52	1.39	1.225	1.295	1.035	1.10	1.31	1.02	0.755	1.52	2.25	0.80	2.73	1.14	1.31	1.34	
$(\varphi = 0.8)$																	
(4) $\frac{Q}{Q_{\text{theoretical}}}$	0.324	0.314	0.333	0.362	0.398	0.386	0.349	0.319	0.407	0.317	0.264	0.407	0.175	0.354	0.323	0.307	
$\frac{Q}{Q_{\text{theoretical}}}$	0.298	0.314	0.340	0.331	0.380	0.365	0.328	0.387	0.451	0.298	0.228	0.434	0.196	0.356	0.326	0.324	
$\frac{Q}{Q_{\text{theoretical}}}$	1.087	1.000	0.980	1.095	1.046	1.057	1.064	0.846	0.902	1.064	1.158	0.938	0.884	0.986	0.985	0.948	1.004
(6) 喷射角	70.4	74.3	69.5	71.8	73.3	75.0	77.3	85.0	74.5	83.6	99.0	82.0	102	78	87	78	
$\frac{\text{喷射角}}{\text{理论喷射角}}$	63.8	81.4	78.3	79.5	73.3	75.2	79.8	72.4	64.7	83.8	94.7	66.7	98.6	75.3	79.8	80.4	
$\frac{\text{喷射角}}{\text{理论喷射角}}$	0.841	0.914	0.889	0.903	1.000	0.997	0.968	1.174	1.150	0.997	1.045	1.230	1.035	1.086	0.971	1.015	

Key: (1) Nozzle No.; (2) Average; (3) Geometric Characteristics; (4) Discharge rate; (5) Ratio of experimental to theoretical; (6) Spray angle.

be approximated with the following relations:

$$\mu = 0.428 A^{-0.619} \quad (5)$$

$$\varphi = 0.630 A^{-0.368} \quad (6)$$

$$\alpha = 65.2^\circ A^{0.307} \quad (7)$$

We obtained these approximate relations by using the least square method on a numerical calculator. In the region $A=0.7 - 4.0$, the results do not differ from those obtained by using equations (2) - (4) by more than 2%.

3. Let us now analyse the operational characteristics of the centrifugal nozzle with an annular outlet. Analogous to the treatment in reference [1], we consider the case of an ideal fluid. Let the radius of the nozzle outlet be r_c , and the radius of the concentric cylinder be r_s so that the actual nozzle outlet cross-sectional area is the annular region bounded by the concentric circles with radii r_c and r_s (Figure 3). There are two possible cases: (1) r_s is less than the radius of the air vortex as calculated from the A value; (2) r_s is larger than this vortex radius. We discuss the cases

separately below:

1) Case of $r_s \leq r_v$ (Figure 3a). Here the cylinder only occupies a part or the whole of the vortex cross-sectional area, and will not affect the flow of the oil. Therefore the discharge coefficient and the spray angle of the nozzle are exactly the same as in the absence of the cylinder. We can use the formulæ (2) - (4) for the simple centrifugal nozzle in our computation. This prediction has been verified by our experiment: from Figure 2, when $(r_s/r_c)^2 \leq 0.38$, the discharge coefficient and the spray angle of the nozzle are independent of $(r_s/r_c)^2$ when the computed value of $(r_v/r_c)^2$ is 0.384, which demonstrates that for $r_s \leq r_v$, the magnitude of r_s does not affect the discharge coefficient and the spray angle of the nozzle. The experimental result of reference [3] agrees with this conclusion.

2) Case of $r_s > r_v$ (Figure 3b). Here the insertion of the central cylinder not only will make the air vortex disappear,

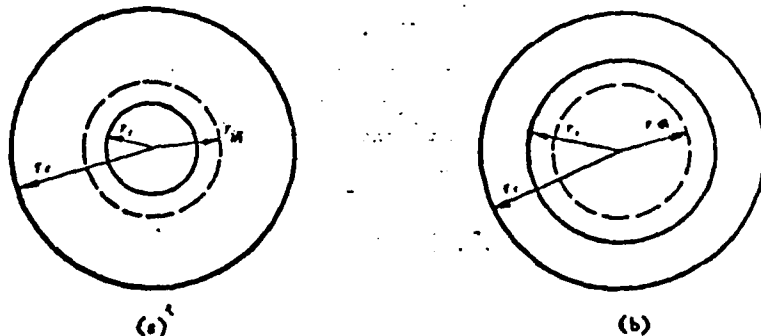


Figure 3. Outlet Cross-section of a centrifugal nozzle with an annular outlet
(a) $r_s < r_v$ (b) $r_s > r_v$

but will also directly affect the area of the oil flow. Let G_s and μ_s respectively represent the flow rate and the discharge

coefficient of the centrifugal nozzle with the annular outlet p_0 be the residual pressure of the fuel oil in the nozzle relative to the ambient medium, γ be the weight of the fuel oil, and g be the gravitational acceleration, then

$$G_s = \mu_s r_s^2 \sqrt{2g \gamma p_0} \quad (8)$$

It is easy to prove with the same method as in reference [1] that: the axial velocity w_a in the cross-sectional area of the outlet is still uniformly distributed, independent of r .

$$\text{Thus, } w_a = \frac{G_s}{\gamma \pi r_s^2 \varphi_s}, \quad \text{where } \varphi_s = 1 - \left(\frac{r_s}{r_v}\right)^2.$$

We notice that the total velocity at the inside boundary r_s of the nozzle's annular outlet (assuming p_s to be the residual static pressure with respect to the ambience at that point) is

$$w_s = \sqrt{w_a^2 + w_t^2} = \sqrt{\frac{2g}{\gamma} (p_0 - p_s)} = \sqrt{\frac{2g}{\gamma} p_0} \sqrt{1 - \frac{p_s}{p_0}}$$

in which the axial velocity $w_a = w_s = \frac{G_s}{\gamma \pi r_s^2 \varphi_s}$, and tangential velocity $w_t = \frac{G_s R}{\gamma \pi r_s^2} = \frac{G_s}{\gamma \pi r_s^2} \frac{A}{\sqrt{1 - \varphi_s}}$. Hence

$$G_s = \gamma \pi r_s^2 \sqrt{\frac{2g}{\gamma} p_0} \frac{\sqrt{1 - \frac{p_s}{p_0}}}{\sqrt{\frac{1}{\varphi_s^2} + \frac{A^2}{1 - \varphi_s}}} \quad (9)$$

Comparing (8) and (9), we know that the discharge coefficient of the centrifugal nozzle with annular outlet when $r_s > r_v$ is

$$\mu_s = \sqrt{1 - \frac{p_s}{p_0}} \sqrt{\frac{1}{\varphi_s^2} + \frac{A^2}{1 - \varphi_s}}$$

For a given nozzle set of and operating conditions, p_0 , A , φ_s are all known quantities. Therefore the key to computing μ_s is the determination of the residual pressure p_s at the surface r_s . Generally speaking, p_s may be a complicated function of φ_s (or r_s). Since at present there is a lack in direct experimental data about p_s , we adopt the method of making all kinds of assumptions on p_s , deriving the corresponding formula for

μ_s and then comparing the different computed results with the experiment to determine which assumption about p_s is more in agreement with reality.

We have made the following three assumptions about p_s :

(1) We assume that the static pressure at $r=r_s$ stays the same before and after introducing the central cylinder. Thus the static pressure p_{s1} at the surface of the cylinder is equal to p_s' , the static pressure at $r=r_s$ in a simple centrifugal nozzle. Analogous to reference [1]

$$p_n - p_s' = \frac{r}{2g} (w_{rB}^2 - w_{rA}^2) = \frac{r}{2g} \left(\frac{G' R}{r \psi f_k} \right)^2 \left(\frac{1}{r_B^2} - \frac{1}{r_A^2} \right) = (\mu A)^2 \left(\frac{1}{1-\varphi} - \frac{1}{1-\varphi_s} \right) p_s$$

whence

$$\text{于是 } \sqrt{1 - \frac{p_n}{p_s}} = \sqrt{1 - (\mu A)^2 \left(\frac{1}{1-\varphi} - \frac{1}{1-\varphi_s} \right)},$$

Substituting into equation (10), we get

$$\mu_n = \frac{\sqrt{1 - (\mu A)^2 \left(\frac{1}{1-\varphi} - \frac{1}{1-\varphi_s} \right)}}{\sqrt{\frac{1}{\varphi_s^2} + \frac{A^2}{1-\varphi}}} \quad (11)$$

(2) We assume that the axial velocity at the nozzle outlet stays constant before and after the introduction of the cylinder, i.e. $w_a/w_a' = 1$. Since

$$\frac{w_s}{w_s'} = \left(\frac{G}{G'} \right) \left(\frac{\varphi}{\varphi_s} \right) = \frac{\mu \varphi}{\mu \varphi_s}$$

then we have

$$\mu_n = \mu \varphi_s / \varphi \quad (12)$$

Substituting equation (12) into (10), we see that this is equivalent to assuming

$$p_n - p_s = \left[1 - \left(\frac{\mu}{\varphi} \right)^2 - \left(\frac{\varphi_s^2}{1-\varphi_s} \right) \left(\frac{4\mu}{\varphi} \right)^2 \right]$$

(3) We assume that the pressure $p_{s3} = 0$ on the surface of the central cylinder at all times, i.e. even $r_s > r_v$, the static pressure on the cylindrical surface is always equal to the ambient pressure. From equation (10) we know

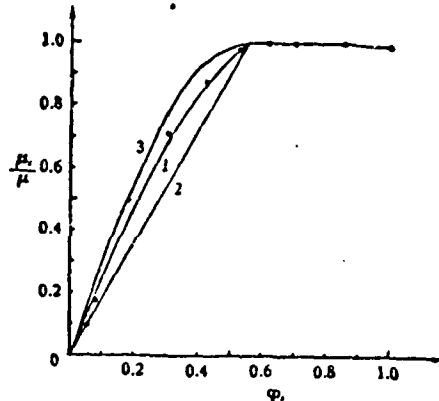
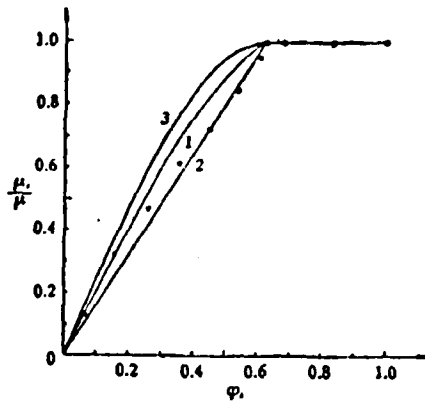
$$\mu_3 = 1 / \sqrt{\frac{1}{\phi_s^2} + \frac{A^2}{1-\phi_s}} \quad (13)$$

All of the equations (11) - (13) derived from the three different assumptions give results in qualitative agreement with the experiment, namely that when $r_s > r_v$, as r_s is increased (ϕ_s is decreased), both the discharge coefficient and the spray angle of the centrifugal nozzle with annular outlet decrease in value (see below). To determine which assumption about p_s is in quantitative agreement with the experiment, we compare the computed results of equation (11) - (13) with experiment. Figure 4 and Figure 5 present the ratio of the computed to the experimental results for the tangential circular hole type nozzle and the tangential rectangular slot type nozzle respectively.

From Figure 4 we can see that for this tangential hole type nozzle, when ϕ_s is large (small blockage), the experimental points follow more closely to the curve calculated from equation (12) and when ϕ_s decreases (blockage increases), the experimental points gradually shift over to the curve of equation (11). From Figure 5 we can see that for the tangential slot type nozzle the experimental points follow more closely the calculated curve of equation (11).

The author of reference [3] changed ϕ_s by installing concentric cylinders of different diameters in the center of the tangential hole type nozzle when he investigated the problem of the interaction between the principal and auxiliary nozzles in a gas-fired turbine. His result showed that the experimental

points follow the curve of equation (12) (Figure 6).



1. Computed from (11) 2 from (12) 3 from (13) Ratio of computed to experimental results

Figure 4. Discharge coefficient of centrifugal nozzle with adjustable outlet area of the tangential hole type.

three $\phi 3.2$ tangential circular holes $A = 1.123$

Figure 5. Discharge coefficient of centrifugal nozzle with adjustable outlet area of tangential slot type.

four rectangular tangential slots 1.87×2.595 $A = 1.575$

Similar to the above, for $r_s > r_v$, the spray angle is calculated from the following equation:

$$\sin\left(\frac{\alpha_s}{2}\right) = \frac{\bar{w}_T}{w_0}$$

where \bar{w}_T is the average tangential velocity at the outlet of the centrifugal nozzle with annular outlet, which we take to be the tangential velocity at $(r_s + r_c)/2$, i.e.

$$\bar{w}_T = \frac{G, R}{\gamma f_1 \psi \left(\frac{r_s + r_c}{2} \right)} = \frac{2A\mu_r}{1 + \sqrt{1 - \varphi_r}} \sqrt{\frac{2g}{\gamma} p_0}$$

The total velocity w_0 when all the pressure energy is transformed into kinetic energy is

$$w_0 = \sqrt{\frac{2g}{\gamma} p_0}$$

Hence

$$\alpha_s = 2 \sin^{-1} \left(\frac{2A\mu_i}{1 + \sqrt{1 - \varphi_i}} \right) \quad (14)$$

Substitute the different μ_s derived from the different assumptions (equation 11 - 13) into equation 14, we get the corresponding formulae for α_s :

$$(1) \quad p_s = p'_s \quad p_s = p'_s \text{ at}, \quad \alpha_s = 2 \sin^{-1} \left(\frac{2A\mu_i}{1 + \sqrt{1 - \varphi_i}} \right) \quad (15)$$

(2) Constant axial velocity before and after introducing the cylinder

$$\alpha_s = 2 \sin^{-1} \left(\frac{2A\mu_i}{1 + \sqrt{1 - \varphi_i}} \right) \quad (16)$$

(3) $p_s = 0$

$$\alpha_s = 2 \sin^{-1} \left(\frac{2A\mu_i}{1 + \sqrt{1 - \varphi_i}} \right) \quad (17)$$

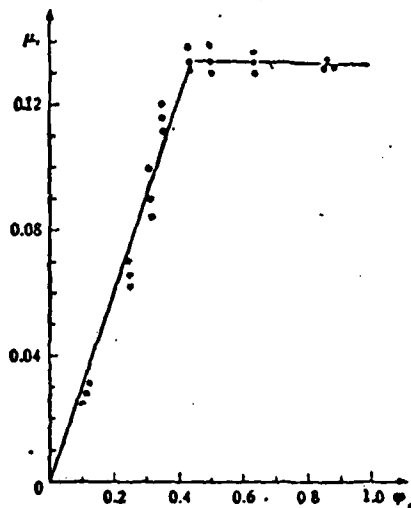


Figure 6. Ratio of discharge coefficient of centrifugal nozzle of tangential orifice type with annular outlet to the computed result from equation 12.
four circular inlet holes

Hence

$$\alpha_s = 2 \sin^{-1} \left(\frac{2A\mu_s}{1 + \sqrt{1 - \varphi_s}} \right) \quad (14)$$

Substitute the different μ_s derived from the different assumptions (equation 11 - 13) into equation 14, we get the corresponding formulae for α_s :

$$(1) \quad p_s = p'_s \quad p_s = p'_s \text{ at}, \quad \alpha_{s1} = 2 \sin^{-1} \left(\frac{2A\mu_{s1}}{1 + \sqrt{1 - \varphi_s}} \right) \quad (15)$$

(2) Constant axial velocity before and after introducing the cylinder

$$\alpha_{s2} = 2 \sin^{-1} \left(\frac{2A\mu_{s2}}{1 + \sqrt{1 - \varphi_s}} \right) \quad (16)$$

(3) $p_s = 0$

$$\alpha_{s3} = 2 \sin^{-1} \left(\frac{2A\mu_{s3}}{1 + \sqrt{1 - \varphi_s}} \right) \quad (17)$$

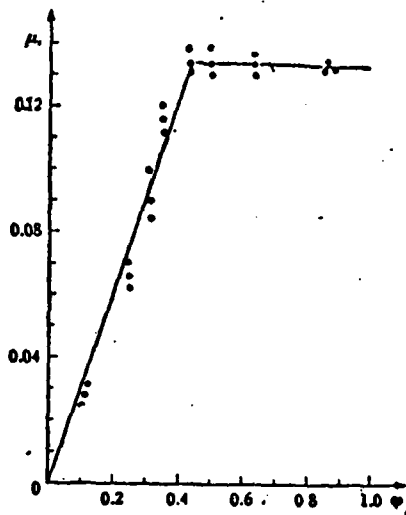
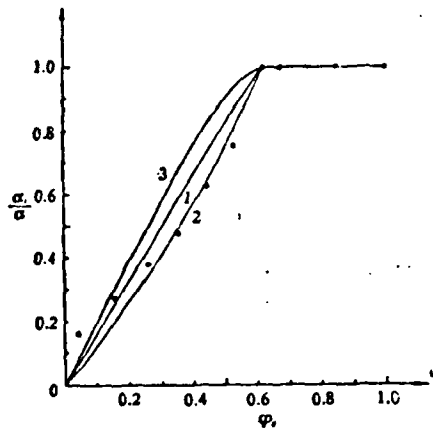


Figure 6. Ratio of discharge coefficient of centrifugal nozzle of tangential orifice type with annular outlet to the computed result from equation 12.

four circular inlet holes

For the tangential hole type and the tangential slot type nozzles that we used in our experiments, the ratio of the experimental result to that computed from equation (15) - (17) are shown separately in Figures 7 and 8. It can be seen that the different formulae all give results in qualitative agreement with experiment, namely that when ϕ_s decreases, the spray angle α_s also decreases. Except for small values of ϕ_s when the error is relatively large, the experimental points for the tangential hole type nozzle are closer to the computed result from equation (16) while those for the tangential slot type nozzle are closer to the computed result from equation (15) (Figure 8). The principal reason why the computed values deviate from experiment for small ϕ_s is that the parts of the nozzle are not truly concentric. The nozzles used in our experiment are used in actual production. There is always some degree of eccentricity between the central pin rod and the orifice. When the blockage is large (or when ϕ_s is small), the spray cone deviates significantly from axial symmetry so that in some directions the spray angle is much larger than that in some other directions. This also affects the discharge characteristics of the nozzle, and may well be what caused the discrepancy in the results for small ϕ_s in Figure 4 and 6.

Thus, for the tangential hold type nozzle, the discharge coefficient (Figure 4 and 6) and the spray angle (Figure 7) both support the assumption that the introduction of the central cylinder does not affect the axial velocity at the nozzle outlet; however, for the tangential slot type nozzle, the discharge rate (Figure 5) and the spray angle (Figure 8) both support the assumption that the static pressure at r_s is not affected by the introduction of the central cylinder. Further investigation is necessary to find out why there is a difference in the regulation characteristics of the two types of nozzles with different structures.



1 is calculated with equation (15); 2 with equation (16);
 3 with equation (17)

Figure 7. The ratio of calculated to experimental values of the spray angle for a centrifugal nozzle of the tangential hole type with adjustable outlet cross-sectional area.

Three 3.2. tangential holes

$$A = 1.123$$

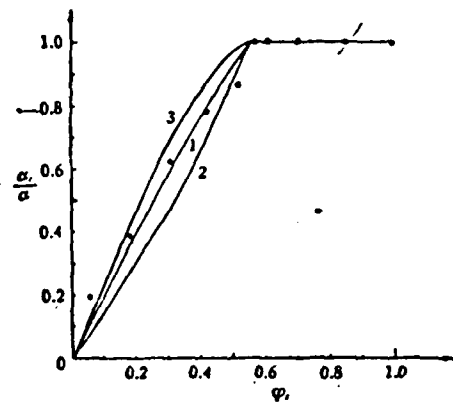


Figure 8. The ratio of calculated to experimental values of the spray angle for a centrifugal nozzle of the tangential slot type with adjustable outlet cross-sectional area.

Four 1.87 x 2.595 rectangular tangential slots.

$$A = 1.575$$

4. In summary, the operational characteristics of the centrifugal nozzle with annular outlet are as follows:

1) When the radius of the central cylinder is not larger than the value of r_v computed from the value of A (equation 1), the introduction of the central cylinder does not affect either the discharge rate or the spray angle of the nozzle. Computations may be carried out with the equations for the simple centrifugal nozzle, equations (2 - 4) (or equations (5 & 7)). For the nozzle with co-axially arranged principal and auxiliary nozzles, the outer diameter of the auxiliary orifice should not be larger than the air vortex of the principal nozzle (calculated from equation 2).

2) When $r_s > r_v$, as ϕ_s decreases (blockage increases), the discharge coefficient and the spray angle of the centrifugal nozzle with annular outlet both decrease. The decrease of the discharge rate is necessary for regulating the fuel rate, but the decrease in the spray angle is usually undesirable. It is just because of this that not too many nozzles with only adjustable nozzle outlet cross-sectional area are used in practice. For such nozzles, the range of the regulation ratio should not be too large, i.e. ϕ_s should not be made too small, so that too small a spray angle may cause an overly concentrated fuel distribution and poor atomization. Within the practical range of regulation ratio, we suggest that equation (12) and (16) be used to compute the discharge rate and the spray angle for a tangential hole type centrifugal nozzle with adjustable outlet cross-sectional area and that equation (11) and (15) be used for the tangential slot type nozzle.

If the nozzle inlet cross-sectional area is also adjusted at the same time when the outlet cross-sectional area is adjusted, then the problem of the changing spray angle when only the outlet cross-sectional area is adjusted may be over-

cone. If designed properly, the spray angle may well remain unchanged when the discharge rate of the nozzle is being adjusted. Some experimental result in this direction was given in reference [4], indicating that this is really an improvement with practical value. However, reference [4] failed to give the correct computational scheme for this case of simultaneously adjusting both the inlet and outlet cross-sectional areas. A slight modification in the computational scheme in our paper should enable us to apply it to this more complicated situation; we need only to consider that in the regulating process, as ϕ_s varies, the inlet cross-sectional area also varies, hence the geometrical characteristic parameter A calculated from equation (1) is now a variable. The effect of this computational scheme will be left for future investigation.

Addendum: The cool state experimental result of the power plant fuel nozzle cited in Table 1 was obtained jointly by the Beijing Central Research Center, Department of Hydroelectricity, the Beijing Thermal Power Generating Station and the Xian Thermal Engineering Research Center. We also cited part of the cool state experimental result on nozzles with adjustable outlet cross-sectional area done at the Capital Steel Forging Plant. Comrades Jin Yongli, Zhang Buzhou, Zui Xiansheng, Zhang Keming, Huang Jiaqi, Yu Zhemin and Wang Shengli also participated in this experiment.

REFERENCES

- [1] Abramovich, G.N. (translated by Zhang Xiuyen) Practical Gas Dynamics, Higher Education Publishing House (1955), 56-62.
- [2] Selected Papers, Topical Conference on Oil Broiler, Chinese Industrial Publishing House (1965), 90-108.
- [3] Kulagin, L.V., Moroshkin, M.Ya. Nozzles for heavy fuel spraying. Mashinostroyeniye, Moscow, 1973, 98-101.
- [4] Akhmedov, R.B., Tsirul'nikov, L.I. Technology for gas and mazut combustion in steam generators. Nedra Press, Leningrad, 1976, 91-98.

DISTRIBUTION LIST
DISTRIBUTED DIRECT TO RECIPIENT

<u>ORGANIZATION</u>	<u>MICROFICHE</u>
A205 DMTRC	1
A210 DMW	1
B344 CIA/OTS-2C	1
C083 ULAMIA	1
C500 UNIVAC	1
C509 BALLISTIC RES LAB	1
C510 R&T LABS/AVRADCOM	1
C511 AVRADCOM	1
C535 AVRADCOM/TSARCOM	1
C539 TRACANA	1
C591 FRC	4
C619 MIA REDSTONE	1
D008 NISC	1
E053 HQ USAF/INER	1
E403 AFSC/INA	1
E404 AFDC/DOF	1
E408 AFWL	1
E410 AD/IND	1
E429 SD/IND	1
P005 DOE/ISA/DDI	2
P050 CIA/OCR/ADD/SD	2
AFIT/LDE	2
FID	1
CIA	1
NIAPHS	1
NIIS	2
LJNL/Cycle L-389	1
NASA/NST-44	1
NSA/1213/TDL	2

